A Novel Power Distribution System Employing State of Available Power Estimation for a Hybrid Energy Storage System

Masoud Masih-Tehrani*, Masoud Dahmardeh

***Abstract*—This paper presents a novel power distribution system (PDS) algorithm to be employed in a hybrid energy storage system (HESS). PDS is responsible to share the demand power between energy storage modules which are battery and ultracapacitor (UC) in this study. The challenge in designing PDS is in assigning the power-share between these modules. A state of available power (SoP) technique is proposed based on the prediction of the power limitations for a pre-defined time frame in the future. Another PDS based on the ultracapacitor state of charge (SoC) is developed. Various design variables are defined which affect the performance of the PDS. Genetic algorithm optimization technique is employed to determine the design variables. The proposed PDS techniques along with an energy storage system (ESS) consisting of a single battery, and a basic PDS system is studied on a 12 kW electric motorcycle during the standard FTP and NYCC driving cycles. Battery lifetime, vehicle range and regenerative braking energy recovery functions for the proposed methods compared with the ESS are improved by 2.6 times, 25 %, and 29 %, respectively. The results suggest that employing the proposed novel PDSs improves the performance of the HESS significantly.**

***Index Terms*—electric vehicle, hybrid energy storage system, lithium battery life, power distribution system, state of available power, ultra-capacitor.**

I. Introduction

CYCLE life is an important parameter while designing the battery of an electric vehicle (EV). Depending on the application, an average cobalt or manganese cathode Li-Ion battery holds about 500 cycles of 80% capacity, before losing 20% of its nominal capacity [1]. After that, the battery should be replaced and the expenses of electricity rise to 0.1 USD/km. Therefore, the current technology makes EVs more expensive than the conventional gasoline vehicles [2]. Hybrid energy storage system (HESS), which is a combination of battery and ultracapacitor (UC), is a popular power storage system [3] for EVs. One of the major advantages of using HESS is moderating the battery current stress to increase its lifetime [4]. However, it is important how the designer choses the modules according to the balance of technological requirements with economic constrains [5].

Recently, HESS is developed for various EV applications, such as electric city bus [6], series hybrid electric bus [7] and fuel cell vehicles [8]. In addition, it is utilized in other applications, such as renewable-energy resources [9], DC microgrids [10] and wind turbines [11].

The power distribution system (PDS) of a HESS determines the performance of the HESS [12]. Many PDSs have been proposed recently, however, this research field is strongly developing. Two simple battery-based and UC-based PDS strategies were presented by Masih-Tehrani et al. [13] and were employed by other research groups [14]. The core idea of these PDSs is providing an assistant system besides the primary storage module, which is battery for the battery-based and UC for the UC-based strategy. These PDSs are very simple, yet efficient in terms of power management. However, their main drawback is that the UC module might reach the fully charged or discharged states very quickly. This results in the waste of regenerated power or the need to provide the whole demand power by the battery alone. Song et al. developed a fuzzy logic controller (FLC) and a model predictive controller (MPC) as PDS for a HESS. They compared their new PDSs with the rule-based controller (RBC) and filtration based controller (FBC) [4]. Some novel PDSs are proposed based on the knowledge of the vehicle driving cycle and dynamic programming optimization approach [15]. The assumption that one knows the future driving condition is not accurate; however, it may be used as an optimal solution for comparing with the performance of other PDSs. Xiao et al. developed a hierarchical control of HESS, composed of both centralized and distributed control, to enhance system reliability [10]. Another approach in designing a PDS is considering the load frequency. In a HESS, high frequency loads are sent to the UC in order to reduce battery strains [16]. By using fast fourier transforms (FFT) or hysteretic current loop (HCL) control, loads can be absorbed by the UC thus avoiding shallow cycles on the battery extending its service life [17]. These studies are suitable for HESS in grid application. Zhang et al. proposed a power distribution strategy considering the path inaccuracy to improve HESS efficiency [18]. The driving conditions are given by advanced technologies in geographic information systems and GPS.

Plett [19] proposed a new state for the battery, *power estimation*. This idea is reported in other studies under different

Manuscript received Month xx, 2xxx; revised Month xx, xxxx; accepted Month x, xxxx.

M. Masih-Tehrani (corresponding author to provide phone: +98-912-3013824; fax: +98-21-73021466; e-mail: masih@iust.ac.ir) and M. Dahmardeh (e-mail: mdahmardeh@iust.ac.ir) are Assistant Professor at School of Automotive Engineering, Iran University of Science and Technology, Tehran, Iran.

names, such as *available power*, *state of power (SoP)* and *State-of-Available-Power (SoAP)*. The prediction time frame depends on the driving condition and is typically between 1 and 20 s [20]. The methods for predicting the battery SoP is divided into three groups: techniques based on the characteristic map [21], dynamic battery model [22] and ANFIS-based technique [23]. Among them, the dynamic battery model is more popular. The proposed models include the Rint, hysteresis, Randles' and resistor-capacitor (RC) network models. The RC model structure provides good dynamic behavior estimation with an acceptable accuracy [24]. For lithium battery packs, various parameters such as temperature distribution, cell-to-cell difference in terms of impedance and capacity either in initial or aged state, should be modeled to have a reliable battery state estimation [25]. To obtain reasonable accuracy, the nonlinear characteristics and dynamic impedance of the batteries are emulated [26]. However, the UC has more linear behavior compared with the battery and therefore, the aging process can be neglected. There are few research works about using SoP for capacitor.

This paper presents a simple PDS (UC-based strategy) initially. Then, the PDS is improved by predicting the state of UC for the next time frame. Moreover, a UC power share governing strategy is proposed based on the UC SoC to improve the PDS of a HESS. The results show that these techniques improve the PDS, HESS and vehicle behaviors.

In the next section, the UC-based power distribution system is introduced. An electric motorcycle is studied as a case study in Section 3. The comparison between simple ESS and a HESS employing a UC-based PDS is presented. In Section 4, the SoP-based power distribution system is proposed and the predicted time frame, as a design variable is optimized. The UC power share governing strategy is developed in Section 5. The new PDS is optimized using genetic algorithm (GA) optimization technique. Comparison of the proposed methods and the basic PDS is presented and the advantages of the proposed methods are elaborated.

II. UC-based Power Distribution System

The PDS based on the UC-based algorithm has two main stages: *UC based PDS* and *Battery and UC limitation check*.

The former follows a simple, yet important rule:

$$P_{UC} = P_{dem} \tag{1}$$

where P_{UC} is the ultracapacitor power and P_{dem} is the HESS demand power. Positive values of power mean that the device is in the discharge mode, while negative values indicate the charge mode. In the next stage (*Battery and UC limitation check*), the UC power limitations are checked. The amount of power that the UC delivers is calculated as follows:

$$P_{UC} = \max(\min(P_{UC}, P_{UC-max}), P_{UC-min}) \tag{2}$$

where P_{UC-max} and P_{UC-min} are the maximum and minimum limitations of the UC power, respectively, which are determined according to the SoC of the ultracapacitor. Calculations of the UC and battery SoCs (SoC_{UC} and SoC_{bat}) are given by Equation (3).

$$SoC_{bat} = 100 \int \frac{-I_{bat}}{C_{bat}},\ SoC_{UC} = 100 \int \frac{-I_{UC}}{C_{UC}} \tag{3}$$

where, I_{UC}/C_{UC} and I_{bat}/C_{bat} are the current/capacitance of the ultracapacitor and battery, respectively. Minus sign in the equation reflects that the positive current is for the discharging mode.

After determining the UC power, the remaining power will be provided by the battery ($P_{bat} = P_{dem} - P_{UC}$). If the ultracapacitor was able to provide all the demand power by itself (considering its limitations), the required battery power would be zero. However, in cases where the UC is unable to supply the demand power, the battery will provide the remaining power. In the last step, power limitations of the battery are checked to ensure that the battery is capable of providing the remaining power. If the remaining power was not within the power capability of the battery, the HESS is unable to provide all the demand power, but a portion of it.

$$P_{bat} = \max(\min(P_{bat}, P_{bat-max}), P_{bat-min}) \tag{4}$$

where $P_{bat-max}$ and $P_{bat-min}$ are the maximum and minimum limitations of the battery power, respectively, which are determined according to the battery SoC, voltage and temperature.

The maximum charge and discharge currents/voltages and other limitations of the UC/battery are given in the datasheet. For some cases, two modes of continuous and pulse are mentioned for the maximum discharge current. To calculate the maximum power (P_{max})/minimum power (P_{min}), the maximum (continuous or pulse) current (I_{max})/minimum current (I_{max}) is multiplied by the terminal voltage (V_{ter}) (Equation (5)). A similar method is employed for the hybrid pulse power characterization (HPPC) method specified by the Partnership for New Generation Vehicles (PNGV) [27], elaborated in [19].

$$P_{max} = I_{max} \times V_{ter},\ P_{min} = I_{min} \times V_{ter} \tag{5}$$

The average current in the last pre-defined time frame determines the allowable current. If the average current is less than the maximum continuous value, the allowable current is the maximum pulse current. Similarly, if the average current is greater than the minimum continuous value, the allowable current is the minimum pulse current. Otherwise, the maximum/minimum allowable current is the maximum/minimum continuous currents.

The terminal voltage is given by Equation (6) and is determined by the open circuit voltage (V_{OC}), current (I) and internal resistance (R_{in}). This equation is valid for both battery and UC, ignoring transient energy storage.

$$V_{ter} = V_{OC} - R_{in} \times I \tag{6}$$

The open circuit voltage is a function of SoC. Fig. 1 plots open circuit voltage of a $LiFePO_4$ battery (solid line) and an ultracapacitor (dashed line) for different values of SoC. As it is shown, the battery shows nonlinear behavior and is similar to an exponential curve. The minimum and maximum values of the voltage for this battery pack are about 60 and 75 volts,

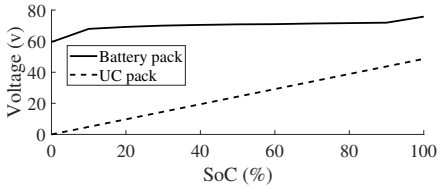

Fig. 1. Open circuit voltage versus SoC for the battery and UC.

respectively. On the other hand, the UC voltage characteristic is linear and the values are in the range of 0 to 50 volts.

III. Case Study: Electric Motorcycle

As a case study, an electric motorcycle is investigated in an FTP standard driving cycle [28].

Main characteristics and specifications of the electric motorcycle and its powertrain are listed in Table I.

TABLE I
Main Specifications of the Electric Motorcycle.

Component	Specification
E-Motorcycle	Total mass (with driver): 250 kg Rolling resistance: 0.003, Drag coefficient: 0.40 Frontal area: 0.60 m^2, Tire radius: 0.24 m
High voltage bus	Voltage: 70 V
Traction Motors	Power: 6 kW (Peak 12 kW) Torque: 70 Nm (Peak 140 Nm)
HESS	Configuration: "UC-battery active topology" [29] DC/DC converter: 12 kW, DC/DC efficiency: 95%
Batteries	286 Lithium $LiFePO_4$ cells (22 cells in series and 13 in parallel) Cell Voltage: 3.3 V (Maximum 3.5 V) Cell Capacity: 2.6 Ah (Totally 33.8 Ah) Cell Continuous Discharge Current: 10 A Cell Peak Discharge Current: 50 A Cell Charge Current: 5 A Cycle life: 2000 at 80 % DoD
Ultra-capacitor	Capacitance: 165 F, Maximum Voltage: 48.6 V Maximum Current (Pulse): 4000 A Maximum Current (Continuous): 150 A

The powertrain model employed in this article is similar to the model reported by Esfahanian et al. [30]. The modeling platform is used for a hybrid electric, a hybrid flywheel and a hybrid hydraulic powertrain simulation and design.

The "UC-battery active topology" HESS configuration is employed [29]. In this type of active parallel configuration, UC is decoupled from the high voltage bus via a DC/DC converter. This is an advantage when a smaller UC is designed. Moreover, by controlling the converter, full UC voltage range can be utilized. Another advantage of this topology is that connecting the battery directly to the high-voltage DC bus keeps a stable DC bus voltage. The DC/DC converter efficiency used in UC-battery power distribution systems is reported between 94% and 99%, for different configurations [31], [32]. However, it is expected that the overall efficiency remains fairly constant at different voltages and powers [33]. In this study, the efficiency of the DC/DC converter is assumed to be 95%.

The generalized life model as a function of the C-rate (ratio of the battery current to its capacity) is proposed by Wang et al. [34] by Equation (7).

$$Q_{\text{loss}} = B\times\exp(-31,700+370.3\times C-\text{rate}/(R\times T))(Ah)^{0.55} \quad (7)$$

where Q_{loss} is the capacity loss in percent, B is the pre-exponential factor and is a function of $C-\text{rate}$ (Table II), R is the gas constant, T is the absolute temperature, and Ah is the Ah-throughput which is expressed as $Ah = (\text{cycle number})\times (DoD)\times$ (full cell capacity).

TABLE II
Values of B with respect to the $C-\text{rate}$ [34].

C-rate	C/2	2C	6C	10C
B values	31,630	21,681	12,934	15,512

The life capacity (Ah) of the 2.6 Ah $LiFePO_4$ battery cell for different battery currents are calculated using Equation (7). The life capacity is defined as the amount of capacity that the battery can provide at a specific current before its capacity reaches 20% [15].

The driving cycle capacity loss ($Q_{\text{loss}-\text{DC}}$) is given by Equation (8) ([15]).

$$Q_{\text{loss}-\text{DC}} = \Sigma\left(I_k \times \mathrm{d}t/3600\right)/(LC(I_k)); \quad k = 0 : t_{\text{DC}} \quad (8)$$

where I_k is the battery current at k^{th} time step and k varies from zero to the driving cycle duration (t_{DC}). $\mathrm{d}t$ is the time step for the calculations and LC is the life capacity and is a function of I_k.

Battery lifetime ($\text{Life}_{bat}(year)$) is calculated according to Equation (9). Since the battery in EV application should be replaced when 20% of its capacity is left, the factor of "0.2" is used. Assuming 8 hours of daily travel itinerary, the denominator of the second fraction shows the average annual working time of an electric motorcycle in seconds.

$$\text{Life}_{bat}(year) = 0.2\frac{C_{bat}}{Q_{\text{loss}-\text{DC}}} \times \frac{t_{\text{DC}}}{3600\times 8\times 250} \quad (9)$$

Essentially, when comparing the lifetime of UC and battery, the former is not a matter of concern and here, it's not modeled. The results of the case study presented here show that the UC is charged and discharged at a maximum number of 4000 cycles per year, in different driving cycles and PDSs. While, numbers of 500,000 cycles to failure is reported for the UC [35] and over than 100,000 cycle life is stated in other reports [29]. Therefore, ignoring UC degradation is reasonable.

Fig. 2 shows the demand power (thick gray line), the battery power (solid black line) and the UC power (dotted line) of a HESS which is equipped with a simple UC-based PDS in the second micro-trip of the FTP driving cycle. As it is shown, a portion of the demand power is provided by the UC, while the battery rests for some seconds. In comparison with a conventional ESS, all of the regenerative braking power is captured and the mechanical brake is not activated.

As presented in Fig. 2, the overall battery power of HESS is smaller than that of ESS. Therefore, the battery life loss is

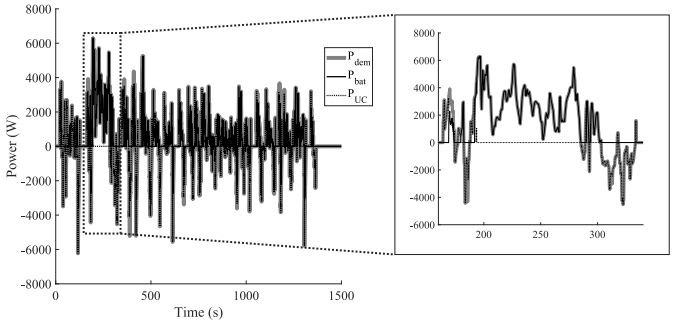

Fig. 2. Electrical power of HESS equipped by simple UC-based PDS for the whole driving cycle and an example interval (inset).

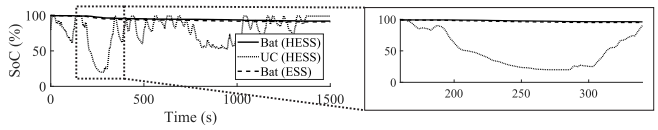

Fig. 3. Variations of the state of charge for ESS/HESS components for the whole driving cycle and an example interval (inset).

improved by adding the UC pack to the ESS. Results show that the battery life loss of a FTP driving cycle for ESS is $3.41 \times 10^{-5}\ Ah$ and for HESS with a simple UC-based PDS is $1.74 \times 10^{-5}\ Ah$ (49% improvement).

Although, the battery power is moderated by adding the UC pack to the ESS, however, performance of the PDS is not perfect, due to the fact that the UC is idle for a considerable amount of time. Fig. 3 shows the SoC of HESS components for the micro-trip shown in Fig. 2.

As it is shown, SoC of the ultracapacitor (dotted line) drops very quickly and therefore is unable to provide power for many seconds. This phenomenon is related to the lower energy capacity of the UC in comparison with the battery. This limitation motivates to progress the current PDS with more sophisticated features to improve performance of the UC in aggressive micro-trips.

As shown in Fig. 3, SoC of the battery in HESS (solid line) drops much more slowly compared with the one for the UC. On the other hand, SoC level of the battery in HESS remains higher (about 9 %) than that of the battery in ESS (about 8 %) and shows an improvement of about 11 %. This is because of the contribution of the ultracapacitor in the HESS and provides a better e-drive range for the HESS compared with the ESS.

IV. SoP-based Power Distribution System

The state of available power predicts power limitations to prevent the energy storage component from violating constrains (maximum or minimum voltage and SoC) during the upcoming seconds. In HESS, the capacity of UC is lower than that of the battery, so the UC is more susceptible to reach the limits. On the other hand, the UC dependency on temperature, state of health and many other complexities are negligible, compared with the ones for the battery. Therefore, SoP of the UC can be defined simply by predicting the SoC and voltage for a specific time frame.

The maximum UC current limits based on the predicted UC SoC for a specific time frame (Δt) are presented by equations (10) and (11) for discharge ($I_{UC-max}^{dis-SoC}$) and charge ($I_{UC-max}^{chg-SoC}$) modes, respectively. The derived equations in this section are similar to the SoP estimation equations developed by Plett [19]. For instance, the difference between Equation (11) and the one presented by Plett is that the Coulombic efficiency factor of the UC is assumed one ($\eta = 1$).

$$I_{UC-max}^{dis-SoC} = \frac{SoC_{UC} - SoC_{UC-min}}{\frac{\Delta t}{C_{UC}}} \tag{10}$$

$$I_{UC-min}^{chg-SoC} = \frac{SoC_{UC} - SoC_{UC-max}}{\frac{\Delta t}{C_{UC}}} \tag{11}$$

In these equations, SoC_{UC-min} and SoC_{UC-max} are the minimum and maximum UC SoC thresholds, respectively. In this article, these values are chosen as 20 % and 98 % for minimum (discharge) and maximum (charge) UC SoC thresholds, respectively.

The maximum UC current limits based on the predicted UC voltages for a specific time frame (Δt) are given by equations (12) and (13) for discharge (I_{UC-max}^{dis-v}) and charge (I_{UC-min}^{chg-v}) modes, respectively. In these equations, V_{OC-UC} is the open circuit voltage of UC during each time frame, V_{UC-min} and V_{UC-max} are the minimum and maximum UC voltage thresholds, respectively. In this article, these values are chosen as 9.7 V and 48.6 V, for minimum (discharge) and maximum (charge) UC voltage thresholds, respectively. $V_{OC-UC-rate}$ is the slope of the open circuit voltage of UC curve versus its SoC (the slope of the dashed line in Fig. 1). R_{in-UC} is the internal resistance of the UC, which is the same for both dis-/charge modes.

$$I_{UC-max}^{dis-v} = \frac{V_{OC-UC} - V_{UC-min}}{\frac{\Delta t}{C_{UC}} \times V_{OC-UC-rate} + R_{in-UC}} \tag{12}$$

$$I_{UC-min}^{chg-v} = \frac{V_{OC-UC} - V_{UC-max}}{\frac{\Delta t}{C_{UC}} \times V_{OC-UC-rate} + R_{in-UC}} \tag{13}$$

Considering the mentioned limits, the maximum UC current limits are determined by equations (14) and (15) for the discharge ($I_{UC-max}^{dis-tot}$) and charge ($I_{UC-min}^{chg-tot}$) modes, respectively. In these equations, three limitation criteria are considered: *catalogue limits*, *predicted SoC* and *predicted voltage*.

$$I_{UC-max}^{dis-tot} = \min\left(I_{UC-max},\ I_{UC-max}^{dis-SoC},\ I_{UC-max}^{dis-v}\right) \tag{14}$$

$$I_{UC-min}^{chg-tot} = \max\left(I_{UC-min},\ I_{UC-min}^{chg-SoC},\ I_{UC-min}^{chg-v}\right) \tag{15}$$

The allowable power based on the SoP is determined by multiplying the maximum current (Equation (14)) and minimum current (Equation (15)) by the predicted voltage value ($V_{ter-UC}(t + \Delta t)$). The maximum (discharge) power and minimum (charge) power based on the SoP are given by equations (16) and (17), respectively.

$$\begin{aligned} P_{UC-max}^{dis-SoP} &= I_{UC-max}^{dis-tot} \times V_{ter-UC}(t + \Delta t) \\ &= I_{UC-max}^{dis-tot}\left(V_{OC-UC}\left(SoC_{UC} - I_{UC-max}^{dis-tot} \times \frac{\Delta t}{C_{UC}}\right) - R_{in-UC} \times I_{UC-max}^{dis-tot}\right) \end{aligned} \tag{16}$$

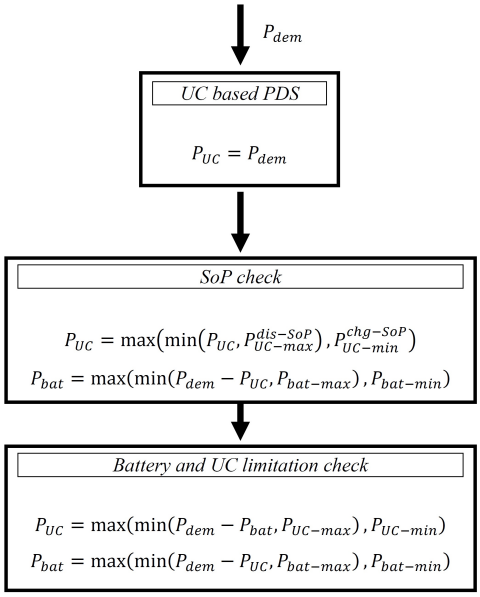

Fig. 4. SoP-based power distribution algorithm.

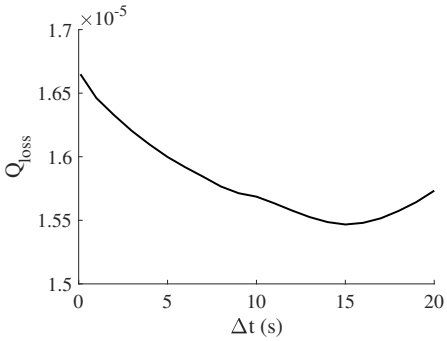

Fig. 5. Battery life loss for HESS with SoP-based PDS versus predicted time period.

$$P_{UC-min}^{chg-SoP} = I_{UC-min}^{chg-tot} \times V_{ter-UC}(t+\Delta t) = I_{UC-min}^{chg-tot}\left(V_{OC-UC}\left(SoC_{UC} - I_{UC-min}^{chg-tot} \times \frac{\Delta t}{C_{UC}}\right) - R_{in-UC} \times I_{UC-min}^{chg-tot}\right) \quad (17)$$

Fig. 4 shows the flow chart of the SoP-based power distribution system. In comparison with UC-based PDS, the *SoP check* stage is added.

Fig. 5 shows the battery life loss during an FTP driving cycle for the HESS employing SoP-based PDS for different values of Δt. Each point of the graph is obtained by simulating a full FTP driving cycle using a specific Δt value and plugging the value into Equations (10) - (17). The results show the dependency of battery life loss on Δt. In this case study, the optimum time frame for the SoP prediction is about 15 s, at which the battery life loss is 1.55×10^{-5} Ah (55 % lower than that of the ESS and 11 % lower than that of the UC-based PDS).

Fig. 6 shows the demand power (thick gray line), the battery power (solid black line) and the UC power (dotted line) of a HESS which is equipped by the SoP-based PDS ($\Delta t = 15$ s)

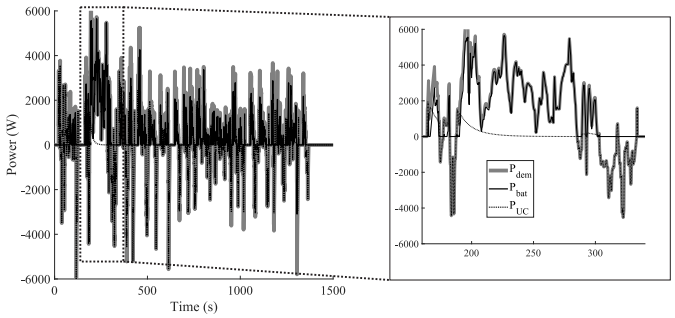

Fig. 6. Electrical power of the SoP-based HESS ($\Delta t = 15$ s); for the whole driving cycle and an example interval (inset).

during the second micro-trip of FTP driving cycle. As it is shown in Figures 2 and 6, power levels of the ultracapacitor for the SoP-based PDS are lower than that of the UC-based one, specially during the early seconds of the driving cycle. However, the UC is more engaged for the SoP-based one and the overall UC power is higher, compared with the UC-based one. Consequently, the overall battery power and life loss for the SoP-based PDS is lower than that of the UC-based one.

V. UC POWER SHARE GOVERNING STRATEGY

As stated, the difference between SoP-based and the UC-based power distribution systems is that the former restricts the UC power consumption before reaching its SoC limits. The design variable of the SoP-based strategy is the predicting time frame (Δt), which can be tuned by a single-variable search optimization method (Fig. 5). In this section, a UC power share governing strategy is proposed based on the ultracapacitor SoC to improve the UC behavior.

Fig. 7 shows the flow chart of the UC power share governing PDS. Compared with the SoP-based power distribution system (Fig. 4), the *UC based PDS* is replaced by the *UC power share governing* block. In the UC-based PDS, all of the demand power is provided by the UC, regardless of its states. However, in the UC power share governing block, a portion of the discharging demand power is provided by the UC. This portion is determined by the power share percent (Sh), which is between 0 to 1 and is a function of UC SoC. When UC SoC is high, the values would be $Sh = 100$ %, otherwise, it is less than 100 %. On the other hand, when the demand power is negative (charging mode), all of the demand power is assigned to the UC ($P_{UC} = P_{dem}$). Although, same as other strategies, limitations of the UC and the battery are checked and if the former is fully charged or if the demanded power is beyond the UC power limitations (during charge or discharge), the remaining (charge or discharge) power is assigned to the battery.

Fig. 8 plots an example of the UC power share (Sh) for different values of UC SoC and essentially determines how the UC is engaged throughout the charge/discharge modes. The goal is to moderate any possible fast discharging of the UC and therefore engaging it more efficiently to improve battery lifetime. Similar strategies are reported in the literature, such as "SoC Recovery" [10] and "SoC to power map" [36]. The

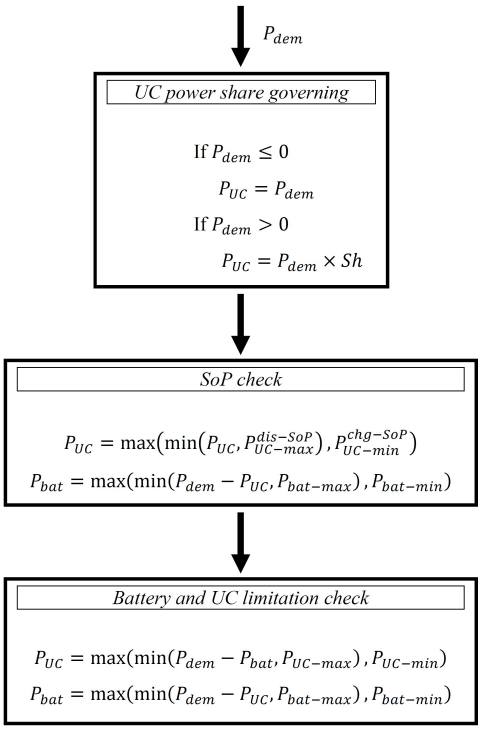

Fig. 7. UC power share governing algorithm.

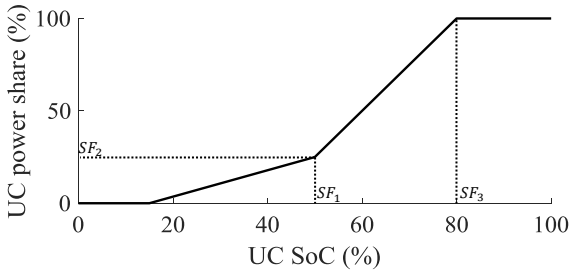

Fig. 8. UC power share percent versus UC SoC.

middle breakpoint is set at 50 % of UC SoC (SF_1) and at 25 % of UC power share (SF_2), while the high breakpoint is fixed at 80 % of the UC SoC (SF_3). If the SoC is greater than SF_3 (UC is almost fully charged), UC provides all of the demanded power ($Sh = 100\%$). This is applied in the first step of Fig. 7, although, it may be limited in the next steps of the algorithm. If the SoC is between SF_1 and SF_3 (moderate SoC), UC provides part of the demanded power. This moderates fast discharging of UC ($SF_2 < Sh < 100\%$). Finally, if the SoC is lower than SF_1 (low SoC), UC provides a small portion of the demanded power ($Sh < SF_2$).

It should be noted that these values are optimized for each case study, along with the predicting time frame (Δt), used during the SoP calculation algorithm.

Results show that the battery life loss for HESS equipped with UC power share governing strategy during an FTP driving cycle is 1.45×10^{-5} Ah which is 57 % lower than that of the ESS, 17 % lower than that of the HESS with UC-based PDS and 6 % lower than that of the HESS with SoP-based PDS. This illustrates the advantages of employing UC power share governing technique in HESS. In the followings, an optimization algorithm is presented to optimize the battery life loss.

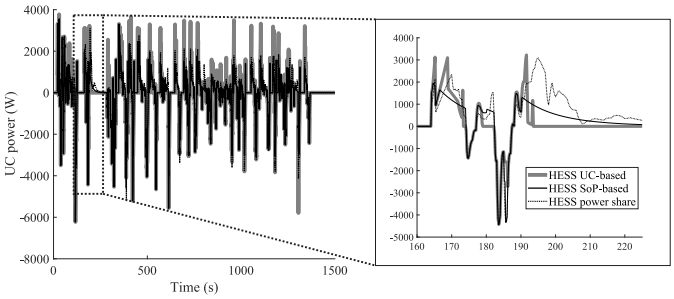

Fig. 9. UC power for an interval during the FTP driving cycle for the whole driving cycle and an example interval (inset).

To solve the battery life loss optimization, genetic algorithm (GA) is utilized [37]. The GA is implemented in MATLAB software to ensure convergence of the solution. Integer programming is selected to reduce the computational cost, while having an acceptable accuracy [38].

Definition of the optimization problem is summarized in Table III.

TABLE III
BATTERY LIFE LOSS OPTIMIZATION PARAMETERS.

Cost function	Battery capacity loss during an FTP driving cycle (Equation (8))
Design variables	Δt: predicting time frame for SoP algorithm SF_1, SF_2 and SF_3: UC SoC and power breakpoints of power share curve (Fig. 8)
Variable bounds	$0\ s \leq \Delta t \leq 30\ s$, $20\ \% \leq SF_1 \leq 50\ \%$ $0\ \% \leq SF_2 \leq 100\ \%$, $51\ \% \leq SF_3 \leq 99\ \%$

The results for this optimization problem are as follows:

$$\Delta t = 12\ s,\ SF_1 = 32\ \%,\ SF_2 = 13\ \%,\ SF_3 = 96\ \%$$
$$Q_{loss-FTP} = 1.43 \times 10^{-5}\ Ah$$

Fig. 9 shows the ultracapacitor power share for an interval during the FTP driving cycle. As shown, for some seconds, power share of the ultracapacitor for the UC-based PDS is greater than that of other ones, specially during 165 s and 190 s. This is not desirable, in terms of power distribution strategy, since the UC power is drained quickly and it would be idle for instances after 195 s. However, total power of the ultracapacitor for the power share governing PDS is greater than that of the SoP-based one, which in turn, is greater than that of the UC-based one. On the other hand, another limitation of the UC-based PDS is that it is unable to deliver all of the regenerative braking energy to the UC at around 185 s, which is not the case for the other two methods. Comparing the three methods, it is suggested that the ultracapacitor operation is most efficient for the power share governing PDS, followed by the SoP-based one, and has less efficiency for the UC-based PDS.

Fig. 10 plots the UC SoC for an interval of the FTP driving cycle. For clarification, the history of the SoC is not shown

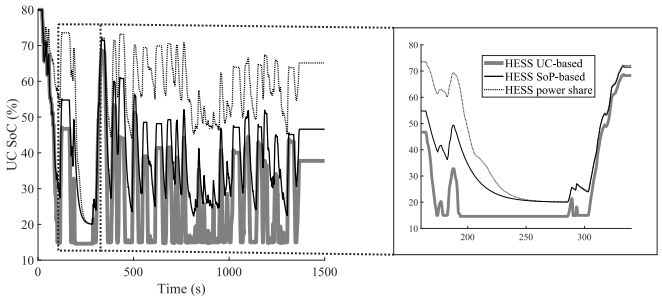

Fig. 10. UC SoC for the whole driving cycle and an example interval (inset).

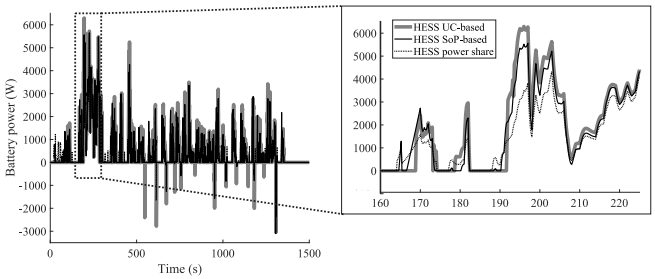

Fig. 11. Battery power consumption for the whole driving cycle and an example interval (inset).

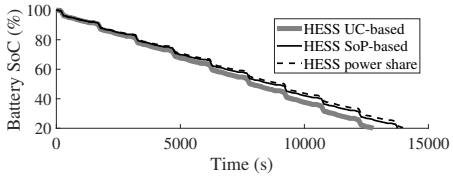

Fig. 12. Battery SoC for the duration of ten FTP driving cycles.

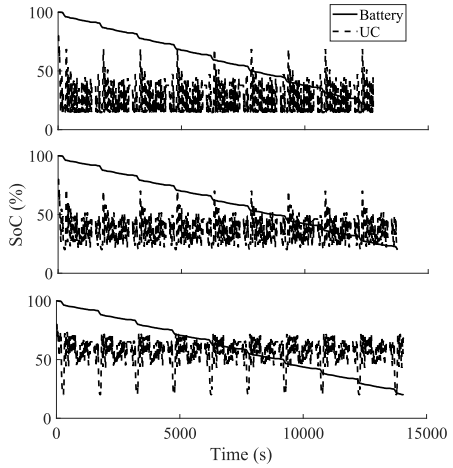

Fig. 13. Battery/UC SoC for the duration of ten FTP driving cycles for UC-based (top), SoP-based (middle) and power share (bottom).

there, therefore, the initial states are different. As discussed in Fig. 9, the UC power management is the most efficient for the power share governing PDS, compared with the other two methods. Therefore, SoC of the ultracapacitor is expected to remain higher than the other two. This is due to the better power management of this method during both dis-/charge modes. As it is shown in Fig. 9, the UC power is drained quickly during the early seconds for the case of UC-based method, which results in the quick drop of UC SoC before 190 s shown in Fig. 10. As can be seen, the level of UC SoC remains low for most of the time during the overall interval. On the other hand, level of UC SoC for the SoP-based PDS is between the other two methods, which is in agreement with the results shown in Fig. 9.

Fig. 11 shows the battery power for an interval during the FTP driving cycle. In this figure, the solid thick gray line is for the UC-based PDS, the solid black line is for the SoP-based PDS and the dotted line is for the power share governing PDS. As discussed, the power share governing PDS provides ultracapacitor with its best performance, following by the SoP-based method. Therefore, as one expects from the results, the overall battery power consumption during the driving cycle should be the highest for the power share governing PDS. This is illustrated in Fig. 11. However, the largest peaks of the battery power are related to the UC-based method, followed by the SoP-based one. This is not desirable considering the battery life. On the other hand, the power share governing PDS moderates the battery power consumption by effectively engaging the ultracapacitor. This results in the lower variations of the battery SoC, compared with the ones for other methods. Variations of the battery SoC are illustrated in Fig. 12 for the duration of ten FTP driving cycles. As shown, the battery SoC reaches its lower limit according to the following order:

1) HESS UC-based PDS
2) HESS SoP-based PDS
3) HESS power share governing PDS.

This shows that the power share governing PDS is able to drive the vehicle for longer ranges, compared with other methods. This is due to the better management of the UC SoC which is shown in Fig. 13. As can be seen, the UC SoC is mostly below 50% for the UC-based case, near 50% for the SoP-based and above 50% for the power share technique. This enables longer driving ranges using the power share technique.

A performance comparison is carried out and listed in Table IV. For this comparison, three items are considered: *Battery lifetime (year)* (calculated by Equation (9)), *Vehicle range (km)* (with a fully-charged battery pack) and *Regenerative energy recovery (Wh)*. As listed in the table, the HESS equipped with power share governing PDS has the highest battery lifetime (8.16 years), vehicle range (133 km) and regenerative energy recovery (132 Wh). The HESS with SoP-based algorithm stands in the second place with battery lifetime of about 7.5 years, vehicle range of 130 km and regenerative energy recovery of about 128 Wh. The UC-based HESS stands in the next places. These results, further illustrate the effectiveness of employing the power share governing PDS for a hybrid energy storage system, compared with the SoP-based HESS or UC-based HESS.

Fig. 14 shows the battery current comparison in an interval of FTP driving cycle. As shown, the battery charging mode for

TABLE IV
PERFORMANCE COMPARISON OF DIFFERENT PDS TYPES IN FTP DRIVING CYCLE.

Power distribution system type	Battery lifetime (year)	Vehicle range (km)	Regen. energy recovery (Wh)
UC-based	6.21	113	125.98
SoP-based	7.00	122	128.23
power share governing	7.56	124	131.59

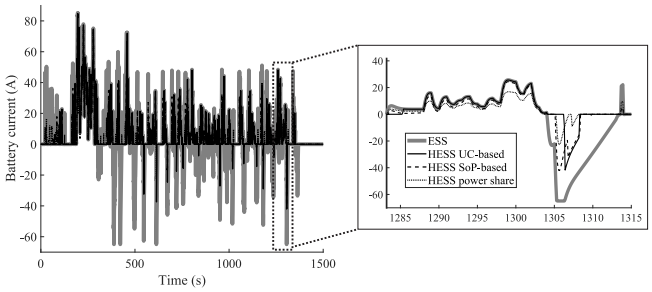

Fig. 14. Battery current during the FTP driving cycle and an example interval (inset).

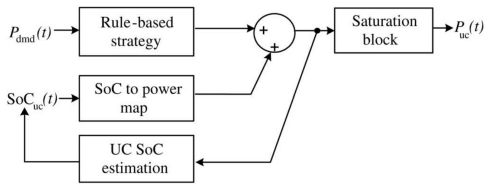

Fig. 15. The rule-based PDS schematic [36].

all PDS strategies is experienced. However, the overall current fed to/drawn from the battery is the most for ESS and is the least for the HESS power share one.

Some other PDSs are introduced in the literature. For example "battery-based PDS" is proposed by Masih-Tehrani et al. [13]. The results show that performance of the battery-based PDS is similar to the ESS case. This is due to the large battery size which provides most, if not all, of the demanded power by itself. In a particular case where the regenerative energy recovery is of concern, the battery-based HESS performs better than the ESS. In this case, the UC-based HESS surpasses the performance of the battery-based HESS. Therefore, adding the ultracapacitor to the battery-based PDS does not help in improving the battery lifetime. This is due to the fact that the primary energy storage is the battery and UC acts as the provider of the extra demanded power, especially in severe braking with high regenerative power. Therefore, the battery current is not moderated significantly for the battery-based HESS.

A rule-based PDS schematic for a HESS is reported in [36]. The algorithm is shown in Fig. 15.

The power distribution strategy is based on a preset value P_{min}. The ultracapacitor power is determined accordingly; if $P_{dem} < 0$, then the UC accepts all regenerative braking power. If $P_{dem} > P_{min}$, then the UC provides part of the discharge

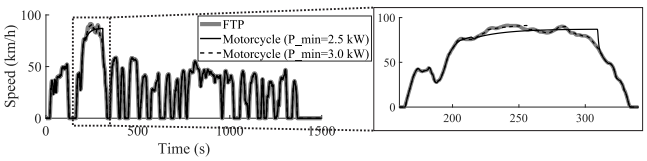

Fig. 16. The FTP driving cycle tracking error using the rule-based PDS; for the whole driving cycle and an example interval (inset).

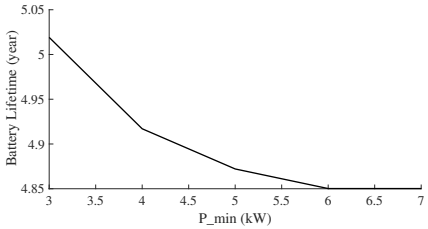

Fig. 17. Battery lifetime of HESS with rule-based PDS in FTP.

power. If $0 < P_{dem} \leq P_{min}$, then the battery provides all discharging power.

For a specific SoC_{UC}, the power map (the "SoC to power map" block shown in Fig. 15) is generated using Equation (18).

$$\begin{aligned} SoC_{UC} &= [0,\ 10,\ 25,\ 50,\ 75,\ 90,\ 100] \\ pwr &= [P_{UC-min}, 0.1P_{UC-min}, 0.025P_{UC-min}, \\ &\quad 0, 0.025P_{UC-max}, 0.1P_{UC-max}, P_{UC-max}] \end{aligned} \tag{18}$$

As can be seen from the algorithm, as P_{min} increases, the battery is engaged more, which in turn decreases lifetime of the battery. Therefore, the value of P_{min} is optimized to improve the battery lifetime. However and on the other hand, there is a minimum value for P_{min}, below which the HESS is unable to provide the demanded power. In order to have a comparison, the mentioned algorithm is applied to the case study of this article. The results show that the minimum acceptable value of P_{min} is about 3 kW. Fig. 16 shows the motorcycle speed in a sample interval of the FTP driving cycle. As can be seen, for the case where $P_{min} = 2.5\ kW$, the motorcycle is unable to follow the FTP driving cycle. However, when $P_{min} = 3\ kW$, the motorcycle has a good cycle tracking. In order to investigate battery lifetime of the rule-based PDS for a HESS in FTP driving cycle, Fig. 17 is plotted. The battery lifetime decreases as P_{min} increases. Even for the best values of the battery lifetime obtained using rule-based PDS, this method lacks the benefits of using HESSs listed in Table IV. This is mainly due to the higher battery usage of the rule-based PDS compared with the UC-based and the proposed strategies.

In order to investigate the effectiveness of the proposed method for other driving cycles, NYCC standard driving cycle [28] is used. The PDS parameters are unchanged and are the same as the ones used for the FTP case. As listed in Table V, the HESS equipped with power share governing PDS has the highest battery lifetime and good vehicle range. This illustrates the effectiveness of the proposed method compared with other HESS algorithms. The value of the regenerative braking

energy recovery is almost similar for all HESS algorithms, which is mainly due to the less aggressiveness of the NYCC cycle compared with the FTP one. This energy is higher for all HESSs compared with the ESS one.

TABLE V
PERFORMANCE COMPARISON OF DIFFERENT PDS TYPES IN NYCC DRIVING CYCLE.

Power distribution system type	Battery lifetime (year)	Vehicle range (km)	Regen. energy recovery (Wh)
UC-based	9.33	470	48.43
SoP-based	11.03	530	48.43
power share governing	12.45	512	48.43

VI. CONCLUSION

A hybrid energy storage system consisting of a battery and an ultracapacitor is presented in this paper. Performance of the system is improved by employing SoP and power share governing techniques. At first, a UC-based strategy is presented, which provides all of the demand power by the UC, until reaching its power limits. The remaining power is then assigned to the battery. Due to the low energy capacity of UC, it becomes fully charged/discharged quickly. Therefore, the battery provides all of the demand power most of the times by itself, which is not desirable. The SoP method is then presented based on the state of available power, which is a prediction of the power limitations for a given time frame in the future. This method engages the UC more efficiently. Finally, a power share governing technique based on the UC SoC is developed. In this method, a portion of the demand power is assigned to the UC, based on its SoC. On the other hand, all of the regenerated power is fed to the UC to capture the power quickly. These PDSs are studied for a 12 kW electric motorcycle during the FTP and NYCC driving cycles. There are four design variables which are optimized using genetic algorithm. The effectiveness of employing power share governing technique over other two methods are summarized as follows:

- Battery lifetime is improved by about 2.6 times and 1.25 times compared with the ESS (battery alone) and the UC-based HESS, respectively.
- Vehicle range is improved by 25 % and 12 % compared with the ESS and the UC-based HESS, respectively.
- Regenerative braking energy recovery is improved 29 % and 5 % compared with the ESS and the UC-based HESS, respectively.

ACKNOWLEDGMENT

This work is supported by Vehicle Dynamical Systems Research Lab and Automotive Engineering Research Center (AERC) of Iran University of Science and Technology (IUST).

REFERENCES

[1] "Sae electric vehicle and plug in hybrid electric vehicle conductive charge coupler," SAE J1772-201602, 2016. [Online]. Available: http://standards.sae.org/j1772_201602.

[2] S. S. Williamson, A. K. Rathore, and F. Musavi, "Industrial electronics for electric transportation: Current state-of-the-art and future challenges," *IEEE Transactions on Industrial Electronics*, vol. 62, no. 5, pp. 3021–3032, 2015.

[3] S. Lukic, J. Cao, R. Bansal, F. Rodriguez, and A. Emadi, "Energy storage systems for automotive applications," *IEEE Transactions on Industrial Electronics*, vol. 55, no. 6, pp. 2258–2267, 2008.

[4] Z. Song, H. Hofmann, J. Li, J. Hou, X. Han, and M. Ouyang, "Energy management strategies comparison for electric vehicles with hybrid energy storage system," *Applied Energy*, vol. 134, pp. 321–331, 2014.

[5] I. Chotia and S. Chowdhury, "Battery storage and hybrid battery supercapacitor storage systems: A comparative critical review," in *2015 IEEE Innovative Smart Grid Technologies - Asia (ISGT ASIA)*, Nov 2015, pp. 1–6.

[6] Z. Song, H. Hofmann, J. Li, X. Han, X. Zhang, and M. Ouyang, "A comparison study of different semi-active hybrid energy storage system topologies for electric vehicles," *Journal of Power Sources*, vol. 274, pp. 400–411, 2015.

[7] M. Masih-Tehrani, M.-R. Hairi-Yazdi, V. Esfahanian, and H. Sagha, "Development of a hybrid energy storage sizing algorithm associated with the evaluation of power management in different driving cycles," *Journal of Mechanical Science and Technology*, vol. 26, no. 12, pp. 4149–4159, 2012.

[8] G. Ren, G. Ma, and N. Cong, "Review of electrical energy storage system for vehicular applications," *Renewable and Sustainable Energy Reviews*, vol. 41, pp. 225–236, 2015.

[9] N. R. Tummuru, M. K. Mishra, and S. Srinivas, "Dynamic energy management of renewable grid integrated hybrid energy storage system," *IEEE Transactions on Industrial Electronics*, vol. 62, no. 12, pp. 7728–7737, 2015.

[10] J. Xiao, P. Wang, and L. Setyawan, "Hierarchical control of hybrid energy storage system in dc microgrids," *IEEE Transactions on Industrial Electronics*, vol. 62, no. 8, pp. 4915–4924, 2015.

[11] W. Li, G. Joós, and J. Bélanger, "Real-time simulation of a wind turbine generator coupled with a battery supercapacitor energy storage system," *IEEE Transactions on Industrial Electronics*, vol. 57, no. 4, pp. 1137–1145, 2010.

[12] A. AllÃ¨gre, A. Bouscayro, and R. Trigui, "Influence of control strategies on battery/supercapacitor hybrid energy storage systems for traction applications," 7-10 September, 2009 2009.

[13] M. Masih-Tehrani, M. Hairi-Yazdi, and V. Esfahanian, "Power distribution development and optimization of hybrid energy storage system," *International Journal of Automotive Engineering*, vol. 4, no. 2, pp. 675–684, 2014.

[14] Z. Amjadi and S. S. Williamson, "Power-electronics-based solutions for plug-in hybrid electric vehicle energy storage and management systems," *IEEE Transactions on Industrial Electronics*, vol. 57, no. 2, pp. 608–616, 2010.

[15] M. Masih-Tehrani, M.-R. Hairi-Yazdi, V. Esfahanian, and A. Safaei, "Optimum sizing and optimum energy management of a hybrid energy storage system for lithium battery life improvement," *Journal of Power Sources*, vol. 244, pp. 2–10, 2013.

[16] R. Karangia, M. Jadeja, C. Upadhyay, and H. Chandwani, "Battery-supercapacitor hybrid energy storage system used in electric vehicle," in *Energy Efficient Technologies for Sustainability (ICEETS), 2013 International Conference on*. IEEE, 2013, pp. 688–691.

[17] H. Jia, Y. Mu, and Y. Qi, "A statistical model to determine the capacity of battery–supercapacitor hybrid energy storage system in autonomous microgrid," *International Journal of Electrical Power & Energy Systems*, vol. 54, pp. 516–524, 2014.

[18] F. Z. S. D. W. W. J. G. C. Zhang, Qiao; Ju, "Power management for hybrid energy storage system of electric vehicles considering inaccurate terrain information," *IEEE Transactions on Automation Science and Engineering*, 2017.

[19] G. L. Plett, "High-performance battery-pack power estimation using a dynamic cell model," *IEEE Transactions on vehicular technology*, vol. 53, no. 5, pp. 1586–1593, 2004.

[20] W. Waag, C. Fleischer, and D. U. Sauer, "Critical review of the methods for monitoring of lithium-ion batteries in electric and hybrid vehicles," *Journal of Power Sources*, vol. 258, pp. 321–339, 2014.

[21] O. Bohlen, J. Gerschler, D. Sauer, P. Birke, and M. Keller, "Robust algorithms for a reliable battery diagnosis-managing batteries in hybrid electric vehicles," in *Proc. The 22nd International Battery, Hybrid and Fuel Cell Electric Vehicle Symposium & Exposition*, 2006.

[22] S. Wang, M. Verbrugge, L. Vu, D. Baker, and J. S. Wang, "Battery state estimator based on a finite impulse response filter," *Journal of The Electrochemical Society*, vol. 160, no. 11, pp. A1962–A1970, 2013.

[23] C. Fleischer, W. Waag, Z. Bai, and D. U. Sauer, "Adaptive on-line state-of-available-power prediction of lithium-ion batteries," *Journal of Power Electronics*, vol. 13, no. 4, pp. 516–527, 2013.

[24] S. Nejad, D. Gladwin, and D. Stone, "A systematic review of lumped-parameter equivalent circuit models for real-time estimation of lithium-ion battery states," *Journal of Power Sources*, vol. 316, pp. 183–196, 2016.

[25] A. Farmann and D. U. Sauer, "A comprehensive review of on-board state-of-available-power prediction techniques for lithium-ion batteries in electric vehicles," *Journal of Power Sources*, vol. 329, pp. 123–137, 2016.

[26] O. König, C. Hametner, G. Prochart, and S. Jakubek, "Battery emulation for power-hil using local model networks and robust impedance control," *IEEE Transactions on Industrial Electronics*, vol. 61, no. 2, pp. 943–955, 2014.

[27] G. Hunt and C. Motloch, "Freedom car battery test manual for power-assist hybrid electric vehicles," *INEEL, Idaho Falls*, 2003.

[28] T. Barlow, *A Reference Book of Driving Cycles for Use in the Measurement of Road Vehicle Emissions: Version 3*, ser. Published project report. IHS, 2009.

[29] E. Chemali, M. Preindl, P. Malysz, and A. Emadi, "Electrochemical and electrostatic energy storage and management systems for electric drive vehicles: State-of-the-art review and future trends," *IEEE Journal of Emerging and Selected Topics in Power Electronics*, vol. 4, no. 3, pp. 1117–1134, 2016.

[30] M. Esfahanian, A. Safaei, H. Nehzati, V. Esfahanian, and M. Masih-Tehrani, "Matlab-based modeling, simulation and design package for eletric, hydraulic and flywheel hybrid powertrains of a city bus," *International Journal of Automotive Technology*, vol. 15, no. 6, pp. 1001–1013, 2014.

[31] P. J. Grbovic, P. Delarue, P. Le Moigne, and P. Bartholomeus, "A bidirectional three-level dc–dc converter for the ultracapacitor applications," *IEEE Transactions on Industrial Electronics*, vol. 57, no. 10, pp. 3415–3430, 2010.

[32] H. Xu, L. Kong, and X. Wen, "Fuel cell power system and high power dc-dc converter," *IEEE Transactions on Power Electronics*, vol. 19, no. 5, pp. 1250–1255, 2004.

[33] A. Kuperman and I. Aharon, "Battery–ultracapacitor hybrids for pulsed current loads: A review," *Renewable and Sustainable Energy Reviews*, vol. 15, no. 2, pp. 981–992, 2011.

[34] J. Wang, P. Liu, J. Hicks-Garner, E. Sherman, S. Soukiazian, M. Verbrugge, H. Tataria, J. Musser, and P. Finamore, "Cycle-life model for graphite-lifepo4 cells," *Journal of Power Sources*, vol. 196, no. 8, pp. 3942–3948, 2011.

[35] C. R. Akli, B. Sareni, X. Roboam, and A. Jeunesse, "Integrated optimal design of a hybrid locomotive with multiobjective genetic algorithms," *International Journal of Applied Electromagnetics and Mechanics*, vol. 30, no. 3, 4, pp. 151–162, 2009.

[36] J. Shen, S. Dusmez, and A. Khaligh, "Optimization of sizing and battery cycle life in battery/ultracapacitor hybrid energy storage systems for electric vehicle applications," *IEEE Transactions on Industrial Informatics*, vol. 10, no. 4, pp. 2112–2121, 2014.

[37] C. R. Houck, J. Joines, and M. G. Kay, "A genetic algorithm for function optimization: a matlab implementation," *NCSU-IE TR*, vol. 95, no. 09, 1995.

[38] T. Yokota, M. Gen, Y. Li, and C. E. Kim, "A genetic algorithm for interval nonlinear integer programming problem," *Computers & industrial engineering*, vol. 31, no. 3, pp. 913–917, 1996.

Masoud Masih-Tehrani received PhD degree in mechanical engineering with major in hybrid energy storage systems (HESS) from University of Tehran (UT), Tehran, Iran, in 2013. He is currently a faculty member and assistant professor at the school of automotive engineering, Iran University of Science and Technology (IUST), Tehran, Iran. His research interests are HESS, hybrid flywheel vehicles, heavy duty vehicles, vehicle suspension systems, and vehicle control systems.

Masoud Dahmardeh received PhD degree in electrical engineering with major in micro-electro-mechanical systems (MEMS) from The University of British Columbia (UBC), Vancouver, Canada, in 2014. He is currently a faculty member and assistant professor at the school of automotive engineering, Iran University of science and technology, Tehran, Iran. His research interests are automotive electronics, microfabrication, micro-electro-mechanical systems, carbon nanotubes (CNT), shape memory alloys (SMA), photonic crystals, active integrated antennas, and radiation.